Li$^+$ ion exchange in H$_2$SrTa$_2$O$_7$ via low temperature acid/base reactions

Chris I. Thomas,[1][2] Thomas W. S. Yip,[3] Serena A. Cussen[1,2] Edmund J. Cussen,[1,2]*

1 Department of Materials Science and Engineering, University of Sheffield, Sheffield, UK

2 Faraday Institution, Harwell Campus, Didcot, UK

3 Department of Pure and Applied Chemistry, The University of Strathclyde, Glasgow, UK

Highlights

- Direct room temperate ion exchange possible allowing the synthesis of, LiHSrTa$_2$O$_7$ from H$_2$SrTa$_2$O$_7$ and LiOH.H$_2$O
- Full exchange to form Li$_2$SrTa$_2$O$_7$ possible at relatively low temperature of 120 °C.
- The defect phase □LiSrTa$_2$O$_{6.5}$ can be formed by dehydrating LiHSrTa$_2$O$_7$

Abstract

Layered materials form a wide range of technologically important ceramics. Within the class of layered materials, ion-exchangeable tantalates have shown great promise. However, the majority of ion exchange methods require large molar excesses of reagents, high temperatures, and by-products or undesired second phases that have to be removed in subsequent reaction steps. Here we show how direct reaction of H$_2$SrTa$_2$O$_7$ with varying quantities of LiOH.H$_2$O at room temperature can exchange protons for Li$^+$. This process does not form a continuous series such as that observed in H$_{2-x}$Li$_x$La$_2$Ti$_3$O$_{10}$, instead forming LiHSrTa$_2$O$_7$ balanced with either unreacted H$_2$SrTa$_2$O$_7$ or LiOH.H$_2$O depending on the initial ratio of H$_2$SrTa$_2$O$_7$ to LiOH.H$_2$O. When H$_2$SrTa$_2$O$_7$ is mixed at room temperature with less than one equivalent of LiOH.H$_2$O it reacts to produce a mixture of H$_2$SrTa$_2$O$_7$ and LiHSrTa$_2$O$_7$. Mixing equimolar amounts of H$_2$SrTa$_2$O$_7$ and LiOH.H$_2$O produces a single phase of LiHSrTa$_2$O$_7$. Room temperature mixing with x LiOH.H$_2$O (1 < x < 2) followed by heating to 120 °C gives a two-phase product mixture of LiHSrTa$_2$O$_7$ and Li$_2$SrTa$_2$O$_7$ and a single phase Li$_2$SrTa$_2$O$_7$ from a reaction with x = 2.

LiHSrTa$_2$O$_7$ can be further dehydrated at 360 °C to form the defect layered perovskite, □LiSrTa$_2$O$_{6.5}$. Materials with Li$^+$ and vacancies on the same crystallographic site often show fast ion conduction but

controllable synthesis has previously proved challenging. The synthesis and degree of exchange is investigated using X-ray powder diffraction data, thermogravimetric analysis and the ionic mobility assessed via *a.c.* impedance spectroscopy. As use of LiOH.H$_2$O has now been shown to directly control ion exchange in both n = 1 and n = 3 (ideal) and n = 2 (distorted) Ruddlesden Popper phases the application of this methodology generally to layered materials is discussed.

Keywords Ion-exchange; Layered-perovskites; Lithiation; Ruddlesden-Popper; Tantalates;

Introduction

Layered materials have found many uses in the modern word from solid lubricants[1] medicines[2] to fertilizers[3]. Of great interest currently is the relatively facile ion mobility observed in many layered materials. In addition to being of scientific interest the ability of certain species e.g. H$^+$[4][5], Na$^+$[6][7], and Li$^+$[8][9] [10] is of crucial importance in a range of fuel cell and battery applications. The Ruddlesden-Popper family of structures, $A_{n+1}B_nX_{3n+1}$ (n = 1 ,2, 3) can be conceptually derived from the related three-dimensional perovskite structure by periodic insertion of a layer of rock salt stoichiometry to give two-dimensional perovskite slabs of finite thickness. The interlayer rock salt sites are typically fully occupied and this limits ion mobility. To counter this, ion exchange and dehydration has been shown to introduce vacancies in a controlled manner e.g. Li$_{2x}$Vac$_{2-2x}$La$_2$Ti$_3$O$_{9+x}$ [11]. The mixing of crystalline LiOH·H$_2$O with the either the *n* = 1 layered perovskite HLaTiO$_4$ or the *n* = 3 H$_2$La$_2$Ti$_3$O$_{10}$ at room temperature gives an ion-exchange reaction, where lithium ions quantitatively replace protons to give the solid-solution series H$_{1-x}$Li$_x$LaTiO$_4$ and H$_{2-x}$La$_2$Ti$_3$O$_{10}$ respectively. [12][11] This reaction is driven not by a stoichiometric excess of lithium cations, but instead by the gain in entropy associated with the liberation of water from the lattice of LiOH·H$_2$O. This entropic change is sufficient to drive endothermic reaction to for Li$_2$MoO$_4$.[13] It is anticipated that this reaction is sufficiently general to allow it to be extended to other protonated layered perovskites. Here we report the results of applying this reaction method to H$_2$SrTa$_2$O$_7$.

The structure of $H_2SrTa_2O_7$ has been extensively studied by Crosnier-Lopez et al. .[14][15] They have shown that the perovskite slabs comprising the framework of this material are not regularly offset by ½$\mathbf{a}$+½$\mathbf{b}$, as is typically observed in the Ruddlesden-Popper family of compounds,[16] but that they can instead be more accurately described by an average of a number of different offsets that are intermediate between eclipsed and staggered arrangements. This variable arrangement between adjacent slabs of perovskite is illustrated schematically in Figure 1, and has the characteristic feature in X-ray powder diffraction profiles, whereby some peaks appear significantly broader than others. These stacking defects have been ascribed to the relative elasticity of the hydrogen bonds across the interlayer region compared to the ionic bonds commonly securing the interlayer alignment,[14] and have prevented a conventional structural characterisation of this material by diffraction methods.

In contrast to the protonated phase, structural investigations into the lithium containing analogue $Li_2SrTa_2O_7$ have revealed arrangements of perovskite slabs that are significantly more regular. This has led to the structure being described as crystallising in the Cmcm space group (Figure 1) rather than the typical I4/mmm for Ruddlesden-Popper n = 2 phases.[17]

These distortions can have crucial impact on technologically important properties and a detailed examination of the crystal structure and properties of $MnSrTa_2O_7$ have identified a novel route to multiferroic phases based on these structures.[18] The particle-size-dependent second harmonic generation of this n = 2 phase indicates a non-centrosymmetric structure and this is confirmed by fitting high resolution neutron powder diffraction in the space group $A2_1am$ rather than Cmcm. The reduction in symmetry is drive by a symmetric tilting of the TaO_6 along the c axis. In the Glazer notation[19] this is described as $a^-a^-c^+$ rather than $a^-a^-c^0$ (in the Amam setting of Cmcm). This reduction in symmetry to the non-centrosymmetric space group permits second harmonic generation and shows that control of the interlayer cation chemistry is likely to be a key component in synthesising these new multiferroic materials.

Partial exchange of Li/H to form $LiHSrTa_2O_7$ can be achieved using either 25 molar excess NH_4Cl at 225 °C under argon or by using dilute HNO_3 heated at 60 °C when the amount of H^+ ions is 'just sufficient'.[20] It is noteworthy that $Li_{2-x}H_xSrTa_2O_7$ solid solution does not appear to be stable instead the x = 0, 1, 2 being only observed phases. It is unclear if this discrete ion exchange proceeds in a random manner or involves a periodic staged replacement of complete layers of protons in an alternating fashion.

Here we describe Li^+ ion exchange of the solid acid $H_2SrTa_2O_7$ has attempted using the same methodology that produced quantitative ion exchange in $HLaTiO_4$ [12,21] and $H_2La_2Ti_3O_{10}$ [11]. X-ray diffraction has been used to monitor exchange of interlayer cations by tracking changes in the unit cell dimensions in the reaction products. These materials have also been examined for their thermal stability, to ascertain whether lithium exchange had occurred and to what extent that this could be achieved and controlled. The method of formation implies facile ion migration through these structures. Moreover, the composition of the phases resulting from subsequent dehydration reactions introduce vacant sites into the interlayer Li^+ sublattice. In order to evaluate ion dynamics and their potential as fast-ion conductors we have collected *a.c.* impedance spectra.

Experimental

Synthesis

The layered perovskite $Li_2SrTa_2O_7$ was prepared by conventional ceramic methods using suitable mixtures of metal carbonates [Li_2CO_3 (0.6425 g, 8.695 mmol), and $SrCO_3$ (1.284 g, 8.695 mmol)] and metal oxides Ta_2O_5 (3.843 g, 8.695 mmol). A 10 wt. % excess of lithium carbonate excess was added to the reagent mixtures to compensate for the volatilisation of this component at high temperature. These reagents were heated in a furnace from room temperature to 500 °C at 1 °C min^{-1}, where they were held for 6 hr before cooling. Two additional firings at 1250 °C for 12 hr, using a 2.5 °C min^{-1} ramp rate were then carried out.

The solid acid $H_2SrTa_2O_7$ was prepared by suspending $Li_2SrTa_2O_7$ (4.800 g (8.342 mmol)) in 480 ml nitric acid (ca. 2 mol dm^{-3}, H$^+$ in 58-fold excess) at 60 °C for 5 d. The exchanged product was then washed with 200 mL of water and recovered by vacuum filtration. The washed product was allowed to dry at room temperature in air.

The replacement of protons with lithium cations in $H_{2-x}Li_xSrTa_2O_7$ was carried out by grinding the solid acid $H_2SrTa_2O_7$ with stoichiometric quantities of $LiOH \cdot H_2O$ under ambient conditions. The reagents (0.1 - 1 g) were ground together for 30 min using a pestle and mortar. The resulting sample was then left to stand in an open-top vial in ambient atmosphere for the reaction to complete over several hours until powder was visibly dry.

X-Ray diffraction

The structures of the protonated and lithium-exchanged phases were analysed by X-ray powder diffraction using a Siemens 500 diffractometer in Bragg-Brentano geometry. The Rietveld method, and Le Bail extractions as implemented in the GSAS suite of programs, [32] were used to analyse the data with pseudo-Voigt and shifted Chebyshev functions describing the peak shape and background, respectively. Layered structures are often susceptible to preferred orientation effects. Diffraction data were collected from samples loaded in a variety of different ways in order to evaluate the impact of sample mounting on diffraction profile, but no significant changes were observed. The March Dollase model of preferred orientation as implemented in GSAS was used to test the data for any such effects. Inclusion of this preferred orientation model in refinements did not improve the quality of fit, and so it was not used in the Rietveld analyses.

Thermal Gravimetric analysis

The thermal stabilities of $H_{2-x}Li_xSrTa_2O_7$, and the lithium-exchanged samples were evaluated using a Perkin Elmer TGA 7 thermal gravimetric analyser. These measurements were carried out under a dynamic atmosphere of dry helium, whereby approximately 30 mg of sample was equilibrated at 40 °C for 5 min before being heated to temperatures of up to 900 °C. Additional experiments involving both the protonated and the lithium-exchanged phases being heated in air and then analysed by X-ray powder diffraction were also employed; these experiments were used to correlate the losses in mass to changes in structure.

Electrochemical impedance spectroscopy

The transport properties of the 1:1 lithium-exchanged samples were assessed by *a.c.* impedance spectroscopy using a Solartron SI 1260 frequency response analyser. These experiments were carried out by pressing approximately 0.2 g of the as-made lithium-exchanged sample under a load of 3 tonnes to give a 10 mm diameter cylindrical pellet approximately 0.7 mm thick. This pellet was attached to two platinum electrodes and heated from room temperature to temperatures of up to 650 °C in air. *a.c.* impedance data were collected from this pellet over the range $0.2 \leq f$ / Hz $\leq 10^6$ on heating over this temperature range.

Results and discussion

The X-ray powder diffraction data of $H_2SrTa_2O_7$ synthesised from acid treatment of $Li_2SrTa_2O_7$,in agreement with Crosnier-Lopez *et al*.[14] could not be fully indexed. However, on the basis of the sharpest and most intense peaks in the range $5 \leq 2\theta \leq 50°$, this diffraction pattern could be partially indexed using a tetragonal cell of dimensions a = 3.84 Å and c = 19.48 Å. With $A_2A'B_2O_7$ stoichiometry the Ruddlesden Popper *n* = 2 phase might be expected for $A_2SrTa_2O_7$ (*A* = Li or H). However, the lithium cations are too small to occupy the 9-coordinate site that is usually associated with A-site cations in the aristotypical Ruddlesden-Popper structure. Instead they inhabit a 4-coordinate site with an unusual, flattened tetrahedral geometry that provides a better match to the bonding requirements of Li^+. These units form an edge-sharing network of LiO_4 units in the interlayer, and so, can be considered to be related to both the Ruddlesden-Popper and Dion-Jacobson structure-types. The formation of this derivative structure when Li sits on the *A* site has been has been confirmed by neutron diffraction studies of both $Li_2SrTa_2O_7$ [17] and $Li_2La_{2/3}Ta_2O_7$.[22] In the case of $Li_2SrTa_2O_7$, rows of TaO_6 octahedra along the [001] direction exhibit an equal tilt in opposite directions relative to non-tilted octahedra in an I4/mmm compound such as $K_2SrTa_2O_7$.[23] This tilting reduces the symmetry of the structure to Cmcm. We note that additional symmetry reduction can arise from displacements of the oxide anions leading to the A2$_1$am structure.[18] This is a subgroup of the Cmcm structure and the subtle displacements of the oxide anions require careful structural characterisation. We simulated the impact of such atomic displacements and the associated reduction in space group symmetry in our materials. The simulations showed that such displacements would make no significant contribution to our data X-ray diffraction data. We follow crystallographic convention in assigning the higher space group symmetry that reasonably fits our diffraction data, but wish to explicitly note that high resolution neutron diffraction data, such as those used to examine $MnSrTi_2O_7$,[18] may identify displacements of the oxide ions that lie beyond the sensitivity of X-ray laboratory diffraction. It should be noted that the crystallinity of these samples has been somewhat degraded by multiple low temperature reactions.

The tilting of these TaO_6 octahedra in the Cmcm structure also gives rise to a cooperative distortion of the LiO_4 tetrahedra, such that a fifth neighbouring oxide anion is brought to within a distance of *ca.* 2.4 Å of the lithium site. Therefore, the coordination of the lithium cation could be considered as intermediate between distorted four-coordinate and five-coordinate square pyramidal. It has been shown that the tilting of these TaO_6 octahedra progressively decreases with heating until, at 230 °C, the structure of $Li_2SrTa_2O_7$ can be described in the aristotypical I4/mmm space group (Figure S1). It appears however that when the Li^+ is replaced with H^+ the interlayer interactions appear to have weakened allowing the perovskite layers to move causing the abundance stacking faults that have been observed previously.[14][15] The replacement of a group one metal with H^+ leading to a reduction in crystallinity has been observed in other layered materials such as $H_{1-x}Li_xLaTiO_4$, [12,21] $HTiNbO_5$[24][25] and $H_2La_2Ti_3O_{10}$[11] but $H_2SrTa_2O_7$ represents the most dramatic result.
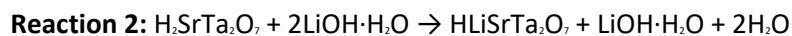
X-ray powder diffraction data collected from a sample of $H_2SrTa_2O_7$ after grinding with one equivalent of LiOH·H_2O showed that a number of the sharp peaks arising from $H_2SrTa_2O_7$ appear to have undergone significant shifts in angle, as illustrated in Figure 2. This is accompanied by the disappearance of a number of broad peaks in the range 25-40° 2θ, such that the diffraction pattern could be fully indexed and refined using an orthorhombic cell (a = 5.537(2) Å, b = 5.549(2) Å, c = 18.7607(13) Å) that is of similar dimensions to that reported for $HLiSrTa_2O_7$.[20]   This indicates that grinding $H_2SrTa_2O_7$ with LiOH·H_2O leads to a significant contraction along the stacking direction of the layered perovskite structure. The mass of the ground sample was also recorded after 5 d, which indicated a loss in mass of ca. 5.2 wt. % that is commensurate with the loss of 1.7 moles of water per formula unit. This loss in mass together with the contraction of the c lattice parameter suggests that reaction (1) had occurred.

Reaction 1: $H_2SrTa_2O_7$ + LiOH·H_2O → $HLiSrTa_2O_7$ + 2H_2O

Additional to the tilting caused by small Li^+ (transforming symmetry from I4/mmm to Cmcm) ordering of the H^+/Li^+ introduces an acentric distortion transforming symmetry further to Ama2. [26]   Heating

the $HLiSrTa_2O_7$ above $\approx$ 200°C causes a reversible phase transition from the orthorhombic Ama2 to the typical Ruddlesden Popper n=2 tetragonal I4/mmm.[26] It should also be noted that transformation of the space group Ama2 to Cmcm leads to a change in the relative orientation of the unit cell axes, whereby the orthorhombic super cell transforms from ($a_p\sqrt{2} \times a_p\sqrt{2} \times c$) to ($c \times a_p\sqrt{2} \times a_p\sqrt{2}$), as illustrated in Figure 3. We used Rietveld refinement of the Ama2 model to examine the XRD data derived from the reaction of $H_2SrTa_2O_7$ with 1 molar equivalent of $LiOH\cdot H_2O$. The final fit obtained to this diffraction pattern is shown in Figure 4.

In an attempt to prepare the fully exchanged compound $Li_2SrTa_2O_7$, a sample of $H_2SrTa_2O_7$ was ground with two equivalents of $LiOH\cdot H_2O$. X-ray powder diffraction data collected from this mixture several days after mixing the reagents could be fitted in a similar manner to the 1:1 data set, as shown in Figure S2. This refinement indicated the presence of an orthorhombic cell (a = 5.536(3) Å, b = 5.546(3) Å, c = 18.7686(13) Å) that is, within error indistinguishable from that of $HLiSrTa_2O_7$ prepared using a 1:1 mixture of reagents, suggesting that reaction (2) had occurred instead.

Reaction 2: $H_2SrTa_2O_7 + 2LiOH\cdot H_2O \rightarrow HLiSrTa_2O_7 + LiOH\cdot H_2O + 2H_2O$

For comparison, the reaction between $H_2SrTa_2O_7$ and half an equivalent of $LiOH\cdot H_2O$ was also carried out. X-ray powder diffraction data were collected from this sample 12 days later and showed an approximately 1:1 mixture of the $H_2SrTa_2O_7$ starting material and the $HLiSrTa_2O_7$ exchanged product, as illustrated in Figure S3, suggesting that reaction (3) had occurred.

Reaction 3: $H_2SrTa_2O_7 + \frac{1}{2}LiOH\cdot H_2O \rightarrow \frac{1}{2}HLiSrTa_2O_7 + \frac{1}{2}H_2SrTa_2O_7 + H_2O$
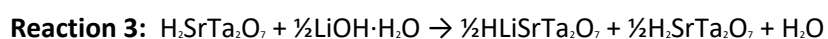
These trial reactions suggest that the $[SrTa_2O_7]^{2-}$ host lattice can only be stabilised by a mixture of protons and lithium cations when they are present in equimolar quantities. However, it was noted that some of the 1:2 samples also gave rise to a number of low intensity peaks that could be indexed as (00l) reflections using the smaller orthorhombic cell of $Li_2SrTa_2O_7$. X-ray powder diffraction data were collected from such a sample after it had been left in ambient atmosphere for a further 5 days,

and showed that the intensities of the peaks arising from $Li_2SrTa_2O_7$ had significantly increased, as illustrated in Figure S4. Therefore, in an attempt to form a monophasic sample of $Li_2SrTa_2O_7$, this mixture was heated at 120 °C in air for a total of 8 d. The resulting sample gave rise to diffraction data that could be fully indexed using the orthorhombic cell of $Li_2SrTa_2O_7$, suggesting that $HLiSrTa_2O_7$ had undergone ion exchange with the remainder of the lithium in the sample. These diffraction data could be fitted using the structural model reported for $Li_2SrTa_2O_7$ in the space group Cmcm [17] as illustrated in Figure 5. The atom positions described by this model could not be refined against the observed data, as similarly encountered when the $[SrTa_2O_7]^{2-}$ model was fitted against the 1:1 data set, but nevertheless provide a reasonable fit to the observed data. Consequently, the atomic coordinates were constrained at the literature values, with the atomic displacement parameters modelled isotropically and fixed at a value of $0.012 Å^2$ for all atoms. In order to provide additional evidence with which to support the reaction schemes proposed, the thermal stabilities of the protonated and lithium-exchanged samples were evaluated. It has previously been shown by Bhuvanesh *et al*. that heating $H_2SrTa_2O_7$ in the temperature range 350-700 °C results in topochemical dehydration of this material to give a defective three-dimensional perovskite, $Sr_{0.5}TaO_3$,[15] as described by reaction (4).

Reaction 4: $H_2SrTa_2O_7 \rightarrow 2Sr_{0.5}TaO_3 + H_2O$
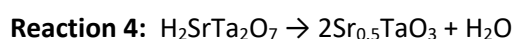
Therefore, a sample of $H_2SrTa_2O_7$ was heated at 360 °C in air for 2 days. X-ray powder diffraction data collected from the resulting sample showed the presence of relatively crystalline peaks that could be indexed using a tetragonal cell (a = 3.925(2) Å and c = 3.983(2) Å) of similar dimensions to that reported for $Sr_{0.5}TaO_3$, as illustrated in Figure S5. The pattern contains a large peak area arising from extremely broadened Bragg peaks along with a broadened peak at approximately 10° 2θ that can be indexed by doubling the c lattice parameter. This suggests that a small quantity of the perovskite with strontium site ordering is still present, as also reported by Bhuvanesh *et al.* The mass of $H_2SrTa_2O_7$ was also monitored during this transformation; thermogravimetric data were collected on heating a sample of $H_2SrTa_2O_7$ at 360 °C under a dynamic atmosphere of dry helium for 2 d, via a 10 °C min^{-1} ramp from

room temperature, and showed a loss in mass of 2.8 wt. %, as illustrated in Figure 6. This mass loss is commensurate with the evaporation of 0.87 moles of water per formula unit, which accounts for the majority of the water produced by reaction (4). Additional thermogravimetric data were collected on heating a sample of $H_2SrTa_2O_7$ from room temperature up to 800 °C at 10 °C min^{-1}, under a dynamic atmosphere of dry helium. This experiment was repeated for a number of separately prepared samples of $H_2SrTa_2O_7$, and, in all cases, indicated a complex mass loss ranging from 3.9 wt. % to 6.8 wt. %, as illustrated in Figure S6.

This mass loss both varies from sample-to-sample, and is in excess of that anticipated from reaction (4). However, all the samples of $H_2SrTa_2O_7$ gave rise to almost identical diffraction patterns. Therefore, although the mass loss recorded on holding a sample of $H_2SrTa_2O_7$ at 360 °C is in agreement with reaction (4), this reaction is not compatible with data recorded over a broader temperature range. This prevents the quantitative interpretation of thermogravimetric data collected from the lithium exchanged samples, which show a more complex mass loss. By comparison, the heat treatment of the 1:1 sample at 360 °C in air for 2 d led to X-ray diffraction data that could be indexed instead using a combination of an orthorhombic cell (a = 18.327(2) Å, b = 5.5562(6) Å and c = 5.5659(7) Å) and a tetragonal cell (a = 3.9321(3) Å and c = 3.9188(7) Å), as illustrated by the LeBail fit in Figure 7(i). The indexing of the orthorhombic cell was performed in the same space group, Cmcm, as used to describe the structure of $Li_2SrTa_2O_7$, rather than that of Ama2, which is used to describe the structure of the $HLiSrTa_2O_7$ parent phase.

These models provide an almost equivalent description of the $[SrTa_2O_7]^{2-}$ sublattice. Given that the protons drive the reduction in symmetry to Ama2, the absence of protons in the heat-treated samples suggests that Cmcm is the more appropriate choice of space group for these dehydrated samples.

After applying the appropriate orientational transformations from Ama2 to Cmcm ($a_p\sqrt{2} \times a_p\sqrt{2} \times c$) to ($c \times a_p\sqrt{2} \times a_p\sqrt{2}$), LeBail analyses indicate the presence of an orthorhombic cell with an a parameter (18.327(2) Å) equivalent to, but significantly shorter than the c parameter (18.7607(13) Å) derived

from the $HLiSrTa_2O_7$ parent compound. The tetragonal cell that is additionally indexed is of similar dimensions to that of the defective perovskite $Sr_{0.5}TaO_3$. These observations suggest that on heating the 1:1 sample at 360 °C, $HLiSrTa_2O_7$ undergoes topochemical dehydration to give a mixture of the defective compounds $\square LiSrTa_2O_{6.5}$ and $Sr_{0.5}TaO_3$, as described by reaction.

Reaction 5: $HLiSrTa_2O_7 \rightarrow (1-x)\square LiSrTa_2O_{6.5} + (\frac{1}{2}x) Li_2O + 2xSr_{0.5}TaO_3 + \frac{1}{2}H_2O$

Scanning electron micrographs published by Gönen *et al.* show that topochemical dehydration of $H_2La_2Ti_3O_{10}$ results in considerable fragmentation of the particles,[27] which both destroys the original platelet morphology and reduces the size of these particles by an order of magnitude. The destructive nature of this approach to vacancy formation should similarly apply to the dehydration of $HLiSrTa_2O_7$, and may therefore account for the formation of $Sr_{0.5}TaO_3$ as a minority product.

In contrast to the dehydration behaviour of $HLiSrTa_2O_7$, the heat treatment of the 1:2 sample under the same conditions led to X-ray diffraction data which could be fully indexed using the orthorhombic cell of $Li_2SrTa_2O_7$. This suggests that the remainder of the protons in the $HLiSrTa_2O_7$ lattice can be replaced with lithium cations when heated at temperatures as low as 120 °C. Additionally, diffraction data collected from the sample heated at 360 °C could be fitted using the structural model of $Li_2SrTa_2O_7$, in a similar manner to data collected from the sample heated at 120 °C, as illustrated in Figure 7(ii). The cell and fit parameters derived from each of the lithium-exchanged phases studied, both as made and after heat treatment at 360 °C, are summarised in Tables S1 and S2, whilst the changes in the lattice parameters are illustrated in Figure 8.

In order to evaluate the potential for fast-ion conduction in the defective layered perovskite $\square LiSrTa_2O_{6.5}$ *a.c.* impedance data were collected from a pellet of each of these materials in air. These experiments initially involved heating a pellet of the $HLiSrTa_2O_7$ parent compound at 360 °C in air for 2 days, to give the dehydrated material. Impedance data were then collected from the resulting pellet up to 650°C. In the temperature range $360 \leq T \leq 550$ °C complex plane plots show a pair of overlapping arcs, as illustrated in Figure 9 for 450 °C. The resistances associated with these arcs were estimated

by fitting the data using an equivalent circuit model consisting of two parallel combinations of a resistor (R) and a constant phase element (CPE). The arc at lower frequency becomes progressively straighter with increasing temperature, and at 600 °C can be described as a tail-like contribution. This tail-like contribution could be modelled using a constant phase element and is attributable to ion-blocking at the electrode interface. The resistance derived from the first arc was used to provide an estimate of the total bulk conductivity of the pellet. The temperature dependence of the total conductivity behaviour exhibited by $\square LiSrTa_2O_{6.5}$ can be fitted using a modified Arrhenius equation, as illustrated in Figure 10, and indicated activation energy of 0.90(10) eV, over the temperature range studied. The conductivity of each of these samples remains low over this temperature range, with typical value of 2.1×10^{-6} S cm^{-1} ($\square LiSrTa_2O_{6.5}$) determined at 450 °C

Although the introduction of vacancies into the Li$^+$ sublattice of $\square LiSrTa_2O_{6.5}$ may be anticipated to enhance ion mobility, the conductivity remains within an order of magnitude of previous reports for the lithium end member, $Li_2SrTa_2O_7$. [28] [29] However, it should be noted that our value of total conductivity is derived from samples containing significant quantities of $Sr_{0.5}TaO_3$, which may be reduce overall ion mobility through the pellet.

Summary

The n = 2 RP phase H2 can be reacted directly with $LiOH.H_2O$ to form $HLiSrTa_2O_7$ and heated at 120 °C to form $Li_2SrTa_2O_7$ or a mixture of these line phases. This provides a sharp contrast to the reaction chemistry observed in the n = 1 and n = 3 systems where the H/Li ratio has been continuously tuned by appropriate control of the stoichiometry of the reaction mixture. The unusual acentric distortion in the n = 2 structure was not observed in either of the n = 1 or n = 3 analogues and the correlation of this distortion with the 1:1 phase $HLiSrTa_2O_7$ suggests that the energetic driver for the formation of line phases in the n = 2 system arises from this distortion. This room temperature reaction pathway thus reproduces the observations from the reaction between molten and excess NH_4Cl with $Li_2SrTa_2O_7$ at 225 °C which afforded preferential stabilisation of the 1:1 product. [18]

These studies suggest that other protonated Ruddlesden-Popper type layered perovskites should be amenable to Li^+ ion exchange when ground with crystalline lithium hydroxide monohydrate possibly requiring modest heating. A synthetic route such as this would complement, as well as be a valuable addition to, the set of reactions by which layered perovskites can be topochemically transformed[30], i.e. at low temperature and in a step-wise manner, to give new materials that are metastable or thermodynamically stable at low temperature. Therefore, the case for this reaction serving as a general route to the Li^+ ion exchange of protonated layered perovskites is made more compelling.

Declaration of Competing Interest

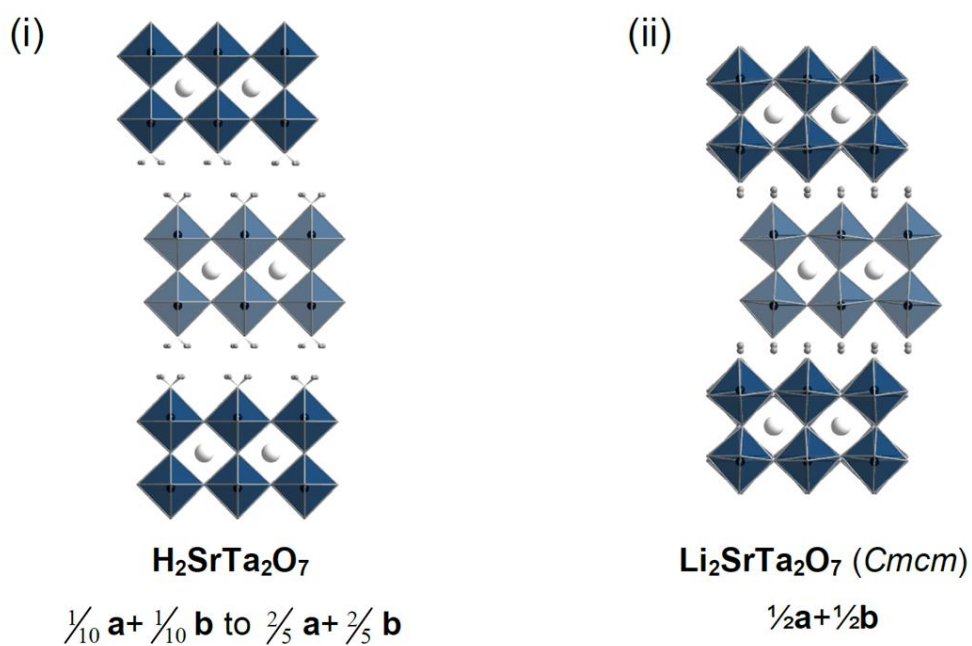The authors declare no competing interest.

Acknowledgements

Figure 1 : Schematic diagram of the proposed structures (i) $H_2SrTa_2O_7$ that has been estimated from stacking fault simulations. [14] Additionally shown is the crystal structures of the lithium analogue (ii) $Li_2SrTa_2O_7$ [17] Interlayer and A-site cations are represented by grey and white spheres respectively, whilst B-site octahedra are indicated by blue units. The lateral offset between adjacent perovskite layers is indicated below each structure.
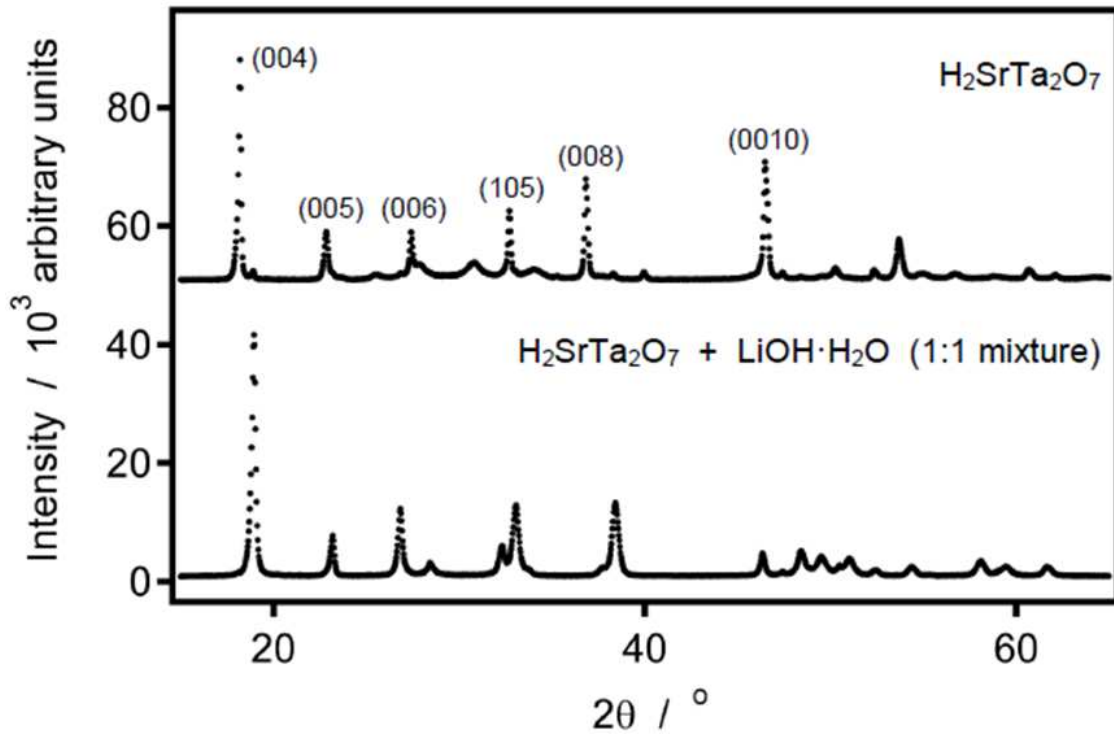
Figure 2 : Observed X-ray diffraction patterns collected from a sample of (i) $H_2SrTa_2O_7$ starting material and (ii) $H_2SrTa_2O_7$ ground with one equivalent of $LiOH.H_2O$ after 5d
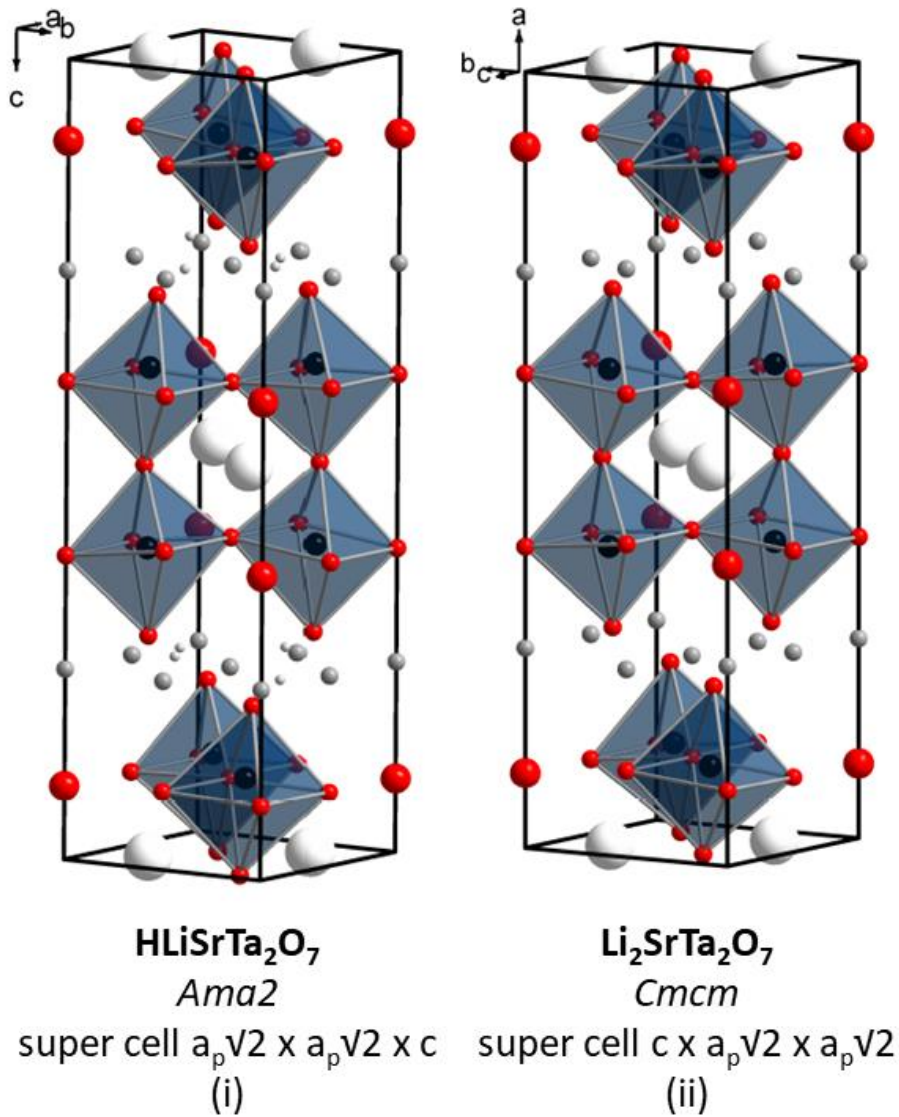
HLiSrTa$_2$O$_7$
Ama2
super cell a$_p$√2 x a$_p$√2 x c
(i)

Li$_2$SrTa$_2$O$_7$
Cmcm
super cell c x a$_p$√2 x a$_p$√2
(ii)

Figure 3 : Crystal structures of (i) HLiSrTa$_2$O$_7$ [20] and (ii) Li$_2$SrTa$_2$O$_7$ [17] described in the space groups Ama2 and Cmcm respectively. Interlayer and A-site cations are represented by grey and white spheres respectively, whilst TaO$_6$ octahedra are indicated by blue units. Note that in the A-centred cell the perovskite layers are stacked along the [001] direction, whereas in the C-centred cell the perovskite layers are stacked along the [100] direction.
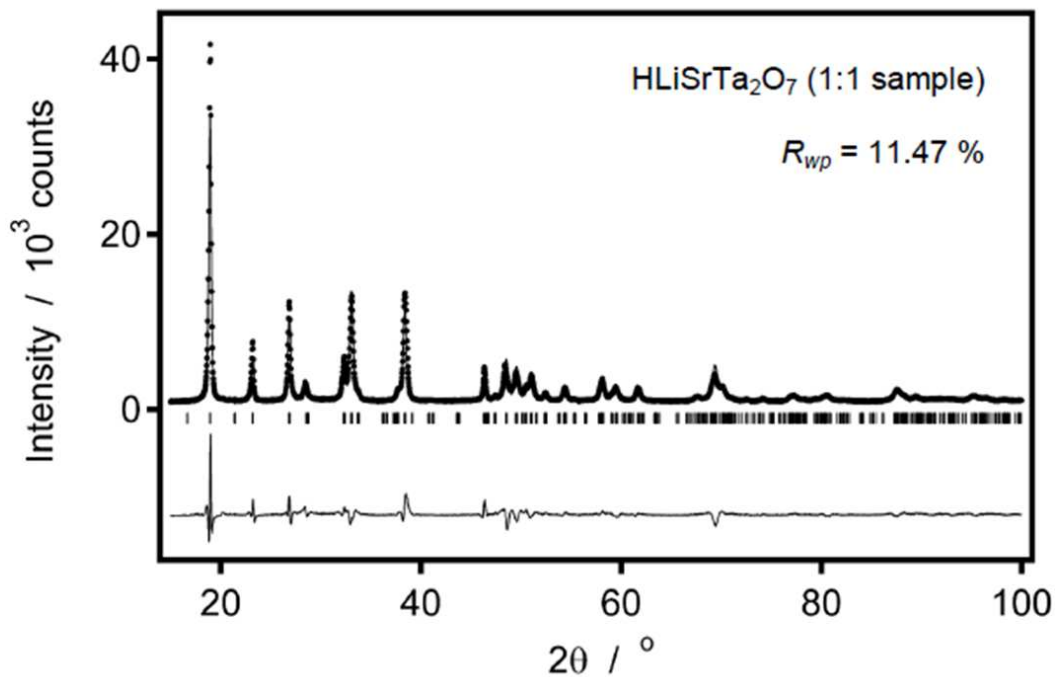
Figure 4 : Observed (dots), calaculated (top line) and difference (bottom line) X-ray powder diffraction patterns from Rietveld analysis of product of a 1:1 reaction. The vertical bars indicate the allowed Bragg reflection positions for $HLiSrTa_2O_7$
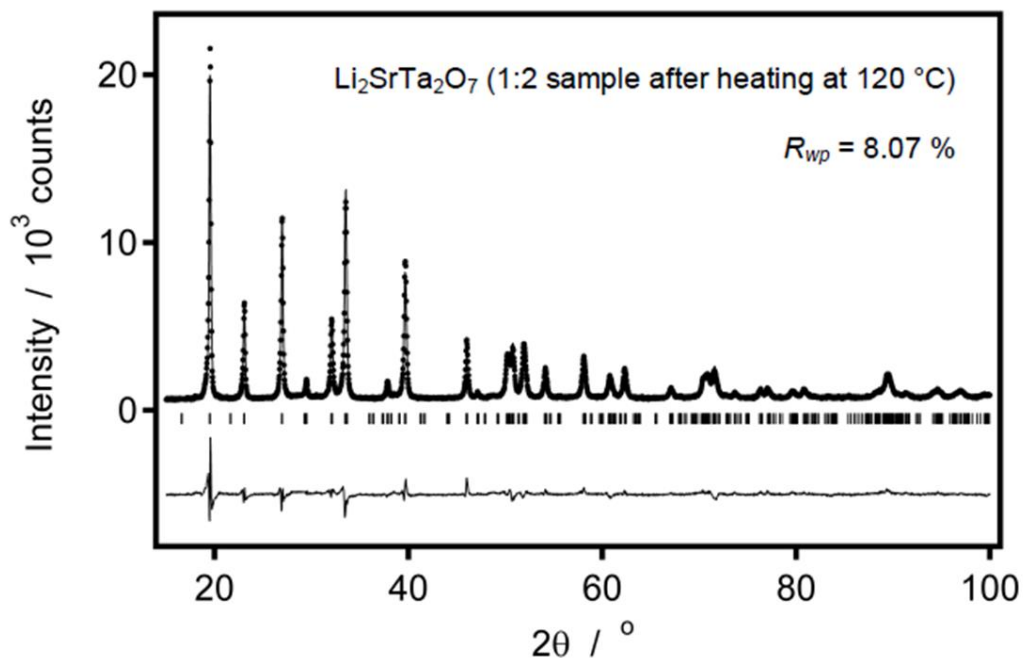

Figure 5 : Observed (dots), calaculated (top line) and difference (bottom line) X-ray powder diffraction patterns for the 1:2 sample after heat treatment at 120 °C in air for a otal of 8 d. The vertical bars indicate the allowed Bragg reflection positions for $Li_2SrTa_2O_7$
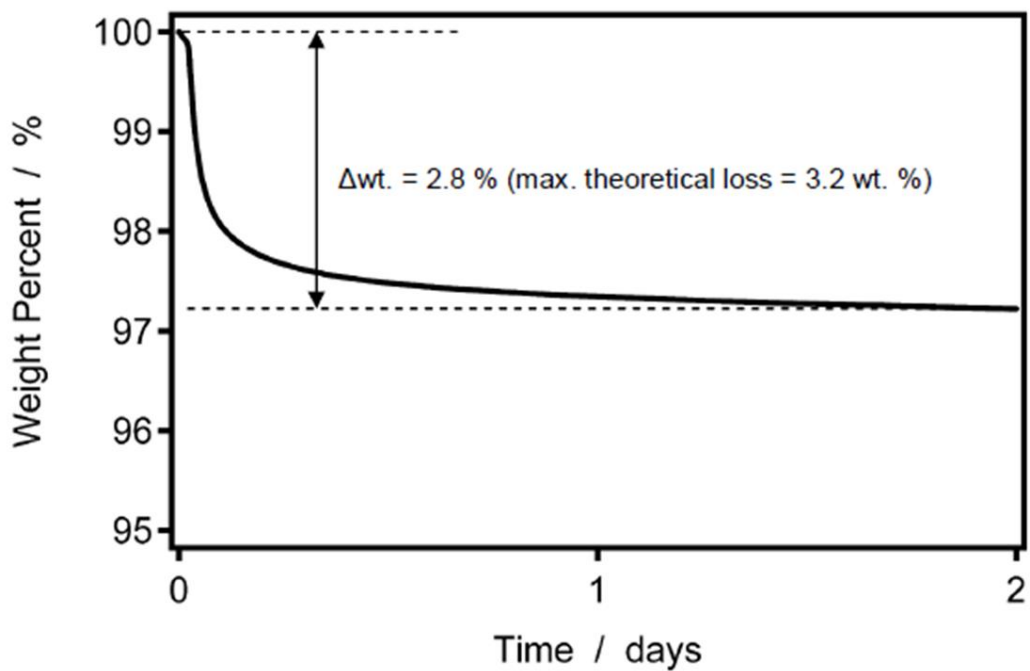
Figure 6 : Thermogravimetric data collected on heating a sample of $H_2SrTa_2O_7$ at 360 °C under a dynamic atmosphere of dry helium for 2 d, via a 10 °C min^{-1} ramp from room temperaure. The maximum loss in mass antipacted from the topochemical dehyradion of $H_2SrTa_2O_7$ is 3.2 wt %)
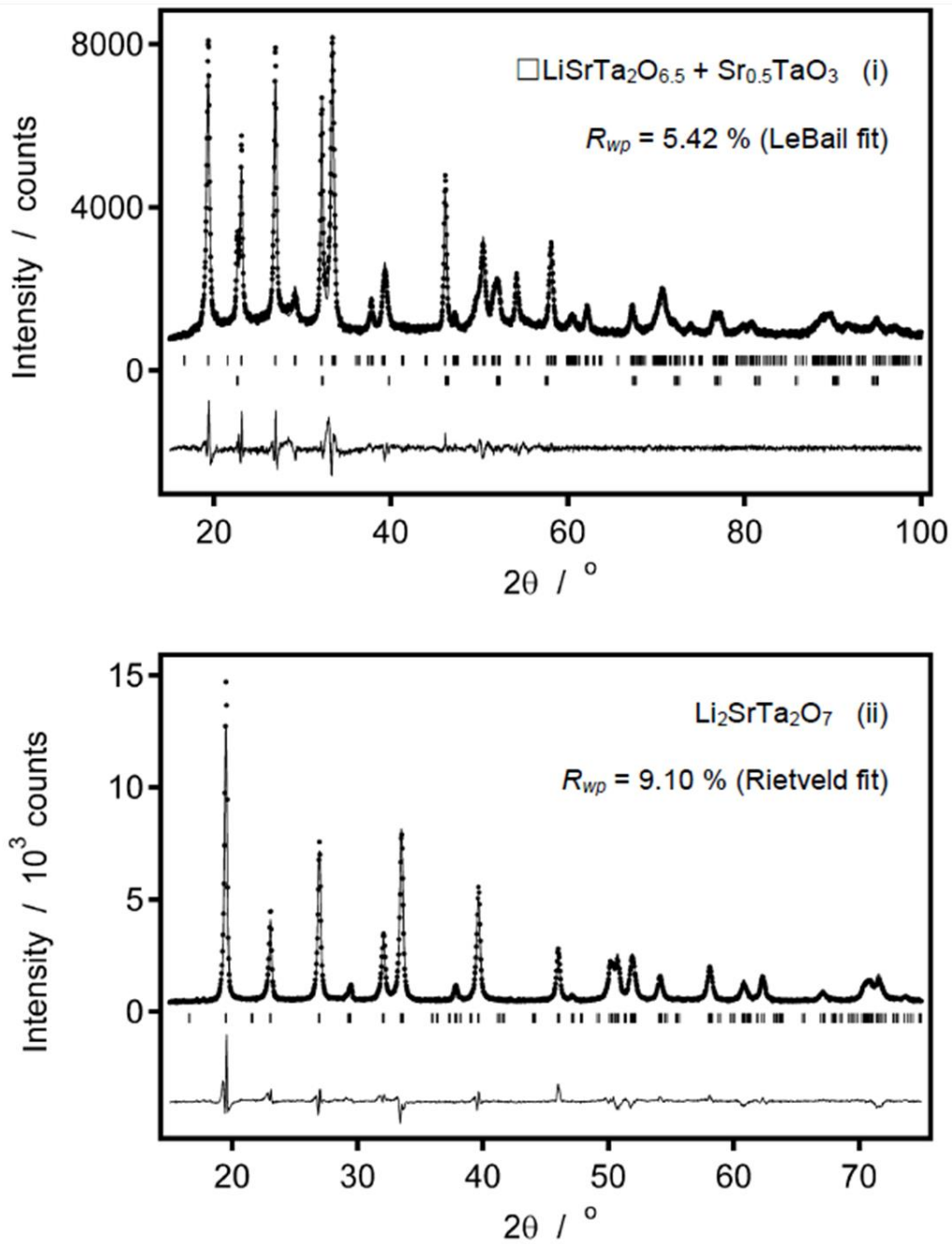
Figure 7 : Observed (dots), calaculated (top line) and difference (bottom line) X-ray powder diffraction patterns for (i) the 1:1 sample and (ii) a 1:2 sample after heat treatment at 360 ° The vertical bars indicate the allowed Bragg reflection positions for an orthorhombic cell in the space group Cmcm, whilst a lower set indicates those allowed for a tetragonal cell in the space group I4/mmm.
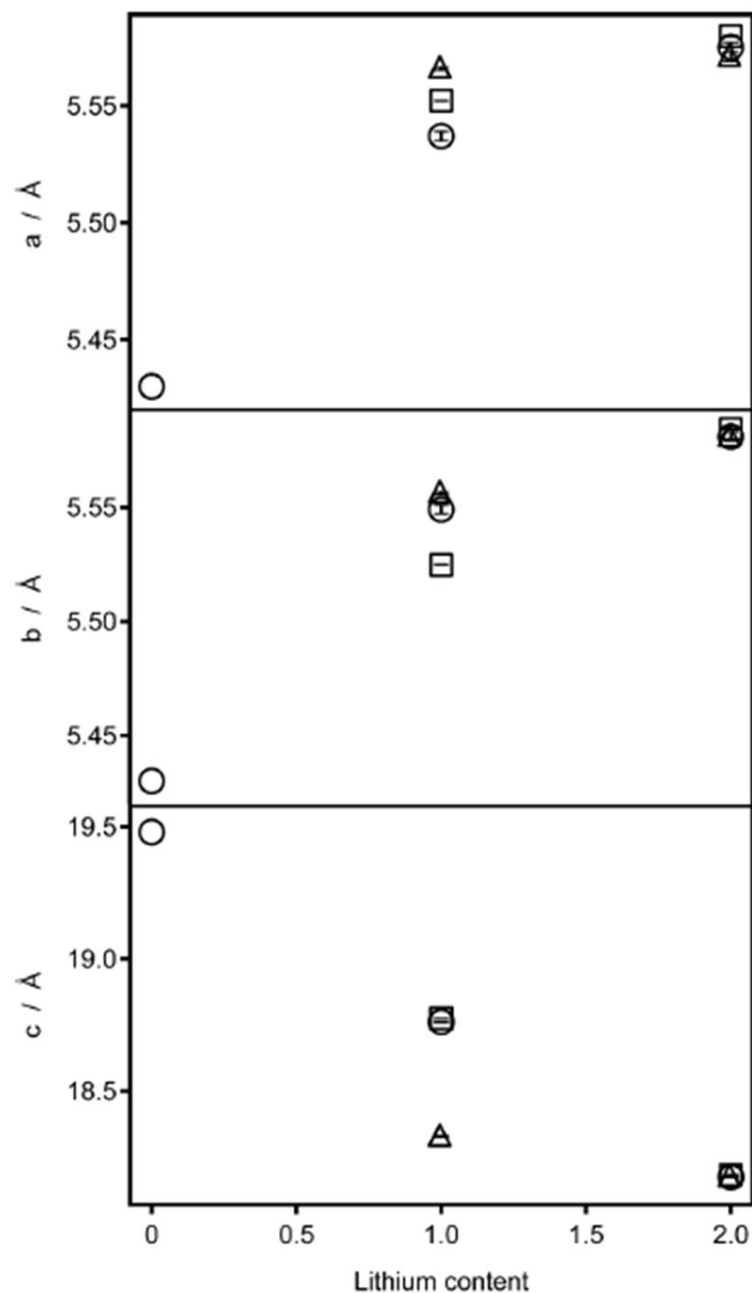
Figure 8 : Lattice parameters of $H_2SrTa_2O_7$* and those of the litium-exchanged samples $H_{Li}SrTa_2O_7$ and $Li_2SrTa_2O_7$ (circles) derived from least-squares refinement against X-ray powder diffraction data. Additionally shown are data collected from the lithium-exchanged samples after heat treatment at 360 °C (triangles), and literature values (squares) for $H_{Li}SrTa_2O_7$ [20] and $Li_2SrTa_2O_7$ [17]. Lattice parameters derived from fits in the space group Cmcm were reoriented from (c x $a_p\sqrt{2}$ x $a_p\sqrt{2}$) to ($a_p\sqrt{2}$ x $a_p\sqrt{2}$ x c) for ease of comparison. *Lattice parameters derived from partial indexing using a tetragonal cell of dimensions a = 3.84 Å and c = 19.48 Å ; the a parameter has been multiplied by $\sqrt{2}$ for ease of comparison.

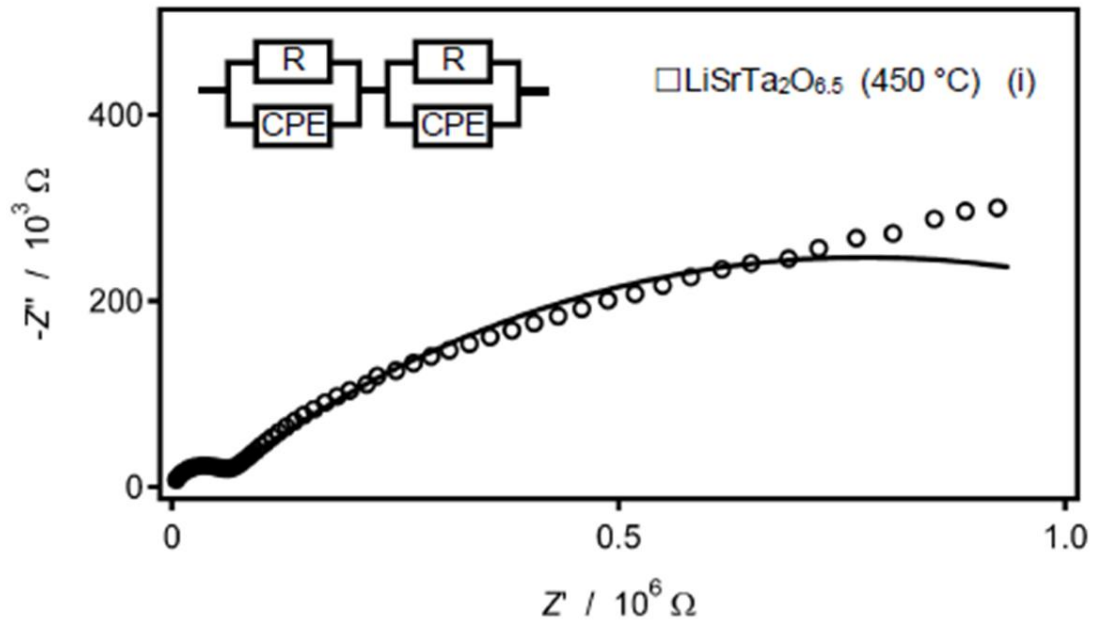**Figure 9** : Complex plane representations of *a.c.* impedance data collected from □LiSrTa$_2$O$_{6.5}$. The conductivity was derived from the equivalent circuit shown.
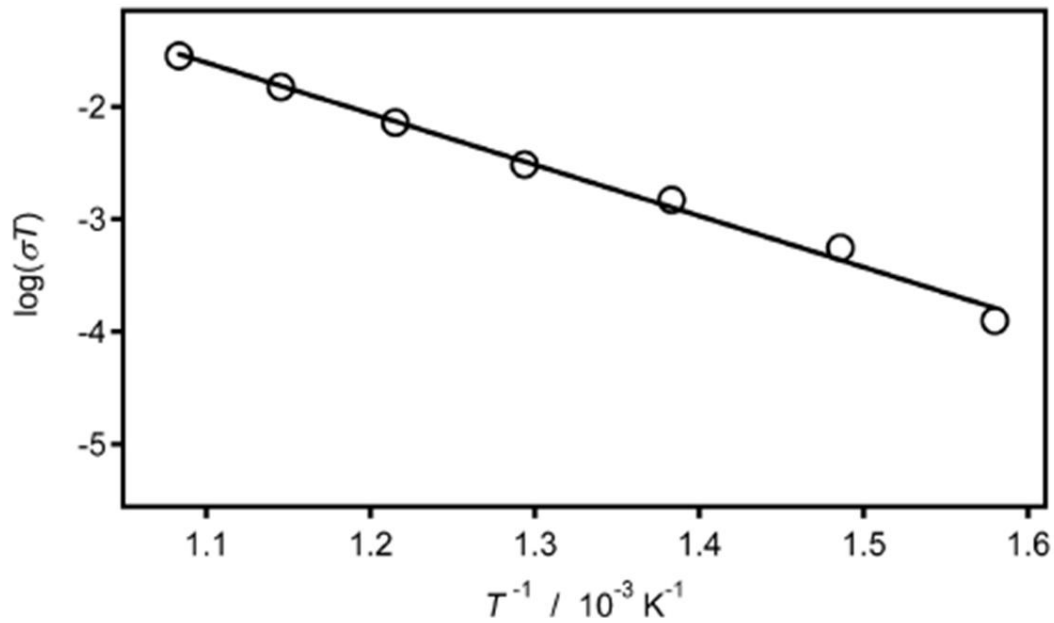

Figure 10 : Plot of total conductivity as a function of temperature for □LiSrTa$_2$O$_{6.5}$ (open circles). The total conductivity was derived from *a.c.* impedance data collected in air. The solid line indicates an Arrhenius fit to the data set.

References

[1]   P. Gonzalez Rodriguez, H. Yuan, K.J.H. van den Nieuwenhuizen, W. Lette, D.J. Schipper, J.E. ten Elshof, Hybrid n-Alkylamine Intercalated Layered Titanates for Solid Lubrication, ACS Appl. Mater. Interfaces. 8 (2016) 28926–28934. doi:10.1021/acsami.6b12716.

[2]   Z. Qin, J. Zhang, H. Chi, F. Cao, Organic--inorganic hybrid nanocomposites based on chitosan derivatives and layered double hydroxides with intercalated phacolysin as ocular delivery system, J. Nanoparticle Res. 17 (2015) 468. doi:10.1007/s11051-015-3275-z.

[3]   S.A.I. Sheikh Mohd Ghazali, M.Z. Hussein, S.H. Sarijo, 3,4-Dichlorophenoxyacetate interleaved into anionic clay for controlled release formulation of a new environmentally friendly agrochemical, Nanoscale Res. Lett. 8 (2013) 362. doi:10.1186/1556-276X-8-362.

[4]   C.E. Tambelli, J.P. Donoso, C.J. Magon, A.C.D. Ângelo, A.O. Florentino, M.J. Saeki, NMR and conductivity study of the protonic conductor $HPb_2Nb_3O_{10} \cdot nH_2O$, Solid State Ionics. 136–137 (2000) 243–247. doi:10.1016/S0167-2738(00)00316-7.

[5]   V. Thangadurai, A.K. Shukla, J. Gopalakrishnan, Proton conduction in layered perovskite oxides, Solid State Ionics. 73 (1994) 9–14. doi:10.1016/0167-2738(94)90258-5.

[6]   S. Das, D. Dutta, R.B. Araujo, S. Chakraborty, R. Ahuja, A.J. Bhattacharyya, Probing the pseudo-1-D ion diffusion in lithium titanium niobate anode for Li-ion battery, Phys. Chem. Chem. Phys. 18 (2016) 22323–22330. doi:10.1039/C6CP04488C.

[7]   N. Van Nghia, P.-W. Ou, I.-M. Hung, Synthesis and electrochemical performances of layered $NaLi_{0.2}Ni_{0.2}Mn_{0.6}O_2$ cathode for sodium-ion batteries, Ceram. Int. 41 (2015) 10199–10207. doi:10.1016/j.ceramint.2015.04.126.

[8]   A. Chakraborty, S. Kunnikuruvan, S. Kumar, B. Markovsky, D. Aurbach, M. Dixit, D.T. Major, Layered Cathode Materials for Lithium-Ion Batteries: Review of Computational Studies on $LiNi_{1-x-y}Co_xMn_yO_2$ and $LiNi_{1-x-y}Co_xAl_yO_2$, Chem. Mater. 32 (2020) 915–952. doi:10.1021/acs.chemmater.9b04066.

[9]   A. Manthiram, A reflection on lithium-ion battery cathode chemistry, Nat. Commun. 11 (2020) 1550. doi:10.1038/s41467-020-15355-0.

[10]   C. Wang, L. Zhang, Z. Zhang, R. Zhao, D. Zhao, R. Ma, L. Yin, Layered materials for supercapacitors and batteries: Applications and challenges, Prog. Mater. Sci. 118 (2021) 100763. doi:10.1016/j.pmatsci.2020.100763.

[11]   C.I. Thomas, T.W.S. Yip, S.A. Cussen, E.J. Cussen, Quantitative ion exchange reactions to form $Li_{2x}Vac_{2-2x}La_2Ti_3O_{9+x}$ defect layered perovskites from $H_2La_2Ti_3O_{10}$ via solid acid/base reaction, J. Solid State Chem. 314 (2022) 123354. doi:10.1016/j.jssc.2022.123354.

[12]   T.W.S. Yip, E.J. Cussen, D.A. MacLaren, Synthesis of $H_xLi_{1-x}LaTiO_4$ from quantitative solid-state reactions at room temperature, Chem. Commun. 46 (2010) 698–700. doi:10.1039/B920837B.

[13]   T.W.S. Yip, E.J. Cussen, C. Wilson, Spontaneous formation of crystalline lithium molybdate from solid reagents at room temperature, Dalt. Trans. 39 (2010) 411–417. doi:10.1039/B908266B.

[14]   M.P. Crosnier-Lopez, J.L. Fourquet, Stacking faults in protonated layered perovskite phases: DIFFaX simulation studies on $H_2SrTa_2O_7$, Solid State Sci. 7 (2005) 530–538. doi:10.1016/j.solidstatesciences.2005.01.015.

[15]   N.S.P. Bhuvanesh, M.-P. Crosnier-Lopez, H. Duroy, J.-L. Fourquet, Synthesis, characterization and dehydration study of $H_2A_{0.5n}B_nO_{3n+1} \cdot xH_2O$ (n = 2 and 3, A = Ca, Sr and B = Nb, Ta) compounds obtained by ion-exchange from the layered $Li_2A_{0.5n}B_nO_{3n+1}$ perovskite materials, J. Mater. Chem. 10 (2000) 1685–1692. doi:10.1039/B000315H.

[16]   R.H. Mitchell, Perovskites modern and ancient, Almaz, Thunder Bay, 2002.

[17]   T. Pagnier, N. Rosman, C. Galven, E. Suard, J.L. Fourquet, F. Le Berre, M.P. Crosnier-Lopez, Phase transition in the Ruddlesden–Popper layered perovskite $Li_2SrTa_2O_7$, J. Solid State Chem. 182 (2009) 317–326. doi:https://doi.org/10.1016/j.jssc.2008.10.029.

[18]   T. Zhu, F. Orlandi, P. Manuel, A.S. Gibbs, W. Zhang, P.S. Halasyamani, M.A. Hayward, Directed synthesis of a hybrid improper magnetoelectric multiferroic material, Nat. Commun. 12 (2021) 4945. doi:10.1038/s41467-021-25098-1.

[19]   A.M. Glazer, The classification of tilted octahedra in perovskites, Acta Crystallogr. Sect. B. 28 (1972) 3384–3392. doi:10.1107/S0567740872007976.

[20]   C. Galven, J.-L. Fourquet, E. Suard, M.-P. Crosnier-Lopez, F. Le Berre, Structural characterization of a new acentric Ruddlesden–Popper layered perovskite compound: $LiHSrTa_2O_7$, Dalt. Trans. 39 (2010) 3212–3218. doi:10.1039/B921017M.

[21]   T.W.S. Yip, E.J. Cussen, Ion Exchange and Structural Aging in the Layered Perovskite Phases $H_{1-x}Li_xLaTiO_4$, Inorg. Chem. 52 (2013) 6985–6993. doi:10.1021/ic4004752.

[22]   F. Le Berre, M.-P. Crosnier-Lopez, Y. Laligant, E. Suard, O. Bohnke, J. Emery, J.-L. Fourquet, Li+ ionic conduction in the layered perovskite $Li_2La_{2/3}Ta_2O_7$, J. Mater. Chem. 14 (2004) 3558–3565. doi:10.1039/B409984M.

[23]   M.-P. Crosnier-Lopez, F. Le Berre, J.-L. Fourquet, The layered perovskite $K_2SrTa_2O_7$: hydration and K^+/H^+ ion exchange, J. Mater. Chem. 11 (2001) 1146–1151. doi:10.1039/B005755J.

[24]   M. Fang, C.H. Kim, T.E. Mallouk, Dielectric Properties of the Lamellar Niobates and Titanoniobates $AM_2Nb_3O_{10}$ and $ATiNbO_5$ (A = H, K, M = Ca, Pb), and Their Condensation Products $Ca_4Nb_6O_{19}$ and $Ti_2Nb_2O_9$, Chem. Mater. 11 (1999) 1519–1525. doi:10.1021/cm981065s.

[25]   C.I. Thomas, M. Karppinen, Intercalation of Primary Alcohols into Layered Titanoniobates, Inorg. Chem. 56 (2017) 9132–9138. doi:10.1021/acs.inorgchem.7b01135.

[26]   C. Galven, D. Mounier, T. Pagnier, E. Suard, F. Le Berre, M.-P. Crosnier-Lopez, Thermal structural characterization of the acentric layered perovskite $LiHSrTa_2O_7$: X-ray and neutron diffraction, SHG and Raman experiments, Dalton Trans. 43 (2014) 14841–14850. doi:10.1039/C4DT01723D.

[27]   Z.S. Gönen, D. Paluchowski, P. Zavalij, B.W. Eichhorn, J. Gopalakrishnan, Reversible Cation/Anion Extraction from $K_2La_2Ti_3O_{10}$: Formation of New Layered Titanates, $KLa_2Ti_3O_{9.5}$ and $La_2Ti_3O_9$, Inorg. Chem. 45 (2006) 8736–8742. doi:10.1021/ic060434g.

[28]   T. Fukushima, S. Suzuki, M. Miyayama, Defect Control and Lithium-Ion Conducting Properties of Layered Perovskite Oxides $Li_2SrTa_2O_7$, Key Eng. Mater. 388 (2009) 69–72. doi:10.4028/www.scientific.net/KEM.388.69.

[29]   S.J. Fanah, F. Ramezanipour, Enhancing the lithium-ion conductivity in $Li_2SrTa_{2-x}Nb_xO_7$ (x = 0–2), Solid State Sci. 97 (2019) 106014. doi:/10.1016/j.solidstatesciences.2019.106014.

[30]   R.E. Schaak, T.E. Mallouk, Perovskites by Design: A Toolbox of Solid-State Reactions, Chem. Mater. 14 (2002) 1455–1471. doi:10.1021/cm010689m.